COMPDYN 2015
5th ECCOMAS Thematic Conference on
Computational Methods in Structural Dynamics and Earthquake Engineering
M. Papadrakakis, V. Papadopoulos, V. Plevris (eds.)
Crete Island, Greece, 25–27 May 2015

A SSI NUMERICAL MODEL FOR LAYERED SOILS USING A BEM-FEM FORMULATION IN TIME DOMAIN

A. Romero, P. Galvín

Escuela Técnica Superior de Ingeniería, Universidad de Sevilla Camino de los Descubrimientos 4109, Sevilla (Spain)
e-mail: {aro,pedrogalvin}@us.es

Keywords: BEM-FEM coupling, Layered half-space fundamental solution, Time domain, Soil-structure interaction

Abstract. *This paper presents a numerical method based on a three dimensional boundary element-finite element coupled formulation in the time domain. The proposed model allows studying soil-structure interaction problems. The soil is modelled with the boundary element method, where the radiation condition is implicitly satisfied in the fundamental solution. Layered half-space Green's function including internal material damping is considered as the fundamental solution because of the influence of soil stratification on soil-structure interaction problems is large. This fundamental solution is computed from the exact expressions for the response in the underlying half-space and from a modal solution for the layers. The finite element method is used to represent the structure. In this paper the proposed method is validated by comparison with analytical and numerical results, and an experimental study is done. Afterwards, the dynamic behaviour of a building subjected to an incident wave field is studied.*

1 Introduction

The response of a soil domain to external loads, earthquakes or moving trains, the response of structures to ground-borne waves, and the response of foundations due to static and dynamic loads are some of the problems where soil-structure interaction (SSI) is important [1]. The Boundary Element Method (BEM) and the Finite Element Method (FEM) can be coupled to study SSI problems rigorously. The semi-infinite character of the soil and the Sommerfeld radiation condition [2] are accurately considered by the BEM [3]. Non-linear dynamic behaviour of structures can be represented from the FEM [4].

BEM models are based on full-space or half-space fundamental solutions. Frequency domain models have been proposed from full-space [3, 5], and from homogeneous and horizontally layered half-space fundamental solutions [6, 7]. Time domain models have been developed by full-space [8] and, recently, from homogeneous half-space fundamental solutions [9, 10]; but time domain models based on layered half-space fundamental solutions have not been presented yet.

SSI problems can be studied by numerical models based on a full-space fundamental solution. In this case, an additional discretization of the free field around the soil-structure interface and the discretization of the soil layers are required. The first previously mentioned numerical problem does not appear using a homogeneous half-space fundamental solution since the free field condition is implicitly satisfied, although the discretization of the soil layers is still necessary. Therefore, the computational effort solution could be dramatically increased. Both numerical problems are solved using a layered half-space fundamental solution: soil discretization is limited to soil-structure interfaces.

Shear, dilatational and Rayleigh waves are not dispersive, and their phase velocities are not frequency dependent in the case of a homogeneous half-space. However, the wave propagation in a layered half-space is dispersive, i.e., the wave propagation velocities depend on the frequency. Therefore the influence of soil stratification on soil-structure interaction problems is large. BEM-FEM frequency domain models are frequently used to study SSI problems. Kaynia and Kausel [11] studied horizontal and vertical stiffness and damping of piles and piles groups in homogeneous and layered half-spaces. Lombaert et al. [12] demonstrated that soil stratification has a considerable influence on both the peak particle velocity and the frequency content of the free field vibrations due to road traffic. Auersch [13, 14] concluded from theoretical and experimental results that the dynamic response of the railway track is strongly influenced by the underlying soil. François et al. [15] and Galvín et al. [16] studied the response of a tunnel embedded in a half-space and the influence of the stratification on the tunnel-soil interaction problem.

The soil stratification is normally disregarded when the time domain formulation is considered. Then, the soil is modelled as an equivalent homogeneous half-space. Rizos and Wang [17] studied the dynamic behaviour of a flexible structure on a rigid foundation. Bode et al. [9] analysed the dynamic response of a railway track due to a moving wheel set by demonstrating the influence of the soil-track interaction. Galvín et al. [18] developed a numerical model for the analysis of vibrations due to train traffic and their effects on nearby structures. Romero et al. [8] analysed the soil-foundation interaction accounting for non-linear soil-structure contact. Galvín and Romero [10] studied a soil-structure interaction problem concerning with a building subjected to different incident wave fields.

The present paper proposes a time domain BEM-FEM methodology using the layered half-space fundamental solution presented by Park and Kausel [19, 20]. This solution is computed

from the exact expressions for the response in the underlying half-space and from a modal solution for the layers. The proposed model allows easily considering soil stratification and material damping.

The paper is organized as follows. Firstly, the layered half-space fundamental solution is discussed. Afterwards, the BEM-FEM formulation based on the previous solution is described emphasising in the integration of the Green's function. Then, the proposed model is numerically verified. Afterwards, an experimental study using the proposed methodology is presented. Finally, the dynamic behaviour of a building subjected to an incident wave field is numerically studied.

2 Layered half-space fundamental solution

In this work, the horizontally layered half-space fundamental solution proposed by Park and Kausel [19, 20] is analysed. The fundamental solution is obtained directly in the time domain. It avoids the numerical problems associated with resonances in the layers. Figure 1 shows schematically the problem geometry, where r is the distance between the observation point and the source, and ϕ is the azimuth angle. The solution for displacements is a second order tensor, $\mathbf{g}(\mathbf{x}, t; \mathbf{x}^i)$, that relates displacements at a point $\mathbf{x}$ due to a load applied at $\mathbf{x}^i$. The tensor component g_{lk} represents the k displacement component due to a load applied according to direction l. A point load with a time variation according to a Heaviside function $H(t)$ is considered in this work. It results advantageous for the analytical computation of the BEM time integrals as can be seen in Section 3.

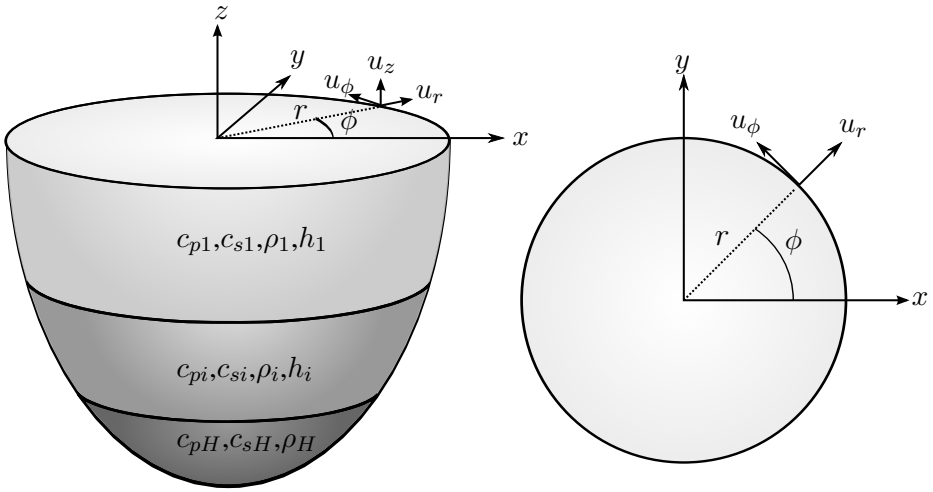

Figure 1: Problem geometry.

The proposed methodology is based on coupling the exact Green's function for a half-space formulated in the wavenumber-time domain [21], with a modal solution for the layers [19, 20]. This topic is briefly summarized in this section.

A homogeneous half-space of mass density ρ_H, damping ratio ξ_H, shear-wave velocity c_{sH}, and dilatational-wave velocity c_{pH} is considered. The displacements in direction k in the half-space at a point due to a load applied at the origin of the cylindrical coordinate system in

direction l are the following [21, 22]:

$$g_{rrH}(r,z,t) = \int_0^\infty \frac{1}{2\pi} H(t) \tilde{G}^{\delta}_{xxH}(k_x,z,t) k J_0(k_x r) dk_x - \tag{1}$$

$$\frac{1}{r}\int_0^\infty \frac{1}{2\pi} H(t) \left[\tilde{G}^{\delta}_{xxH}(k_x,z,t) - \tilde{G}^{\delta}_{yyH}(k_x,z,t)\right] J_1(k_x r) dk_x \tag{2}$$

$$g_{rzH}(r,z,t) = \frac{-1}{i}\int_0^\infty \frac{1}{2\pi} H(t) \tilde{G}^{\delta}_{xzH}(k_x,z,t) k_x \frac{\partial}{\partial k_x r} J_0(k_x r) dk_x \tag{3}$$

$$g_{\theta\theta H}(r,z,t) = -\int_0^\infty \frac{1}{2\pi} H(t) \tilde{G}^{\delta}_{yyH}(k_x,z,t) k_x J_0(k_x r) dk_x - \tag{4}$$

$$\frac{1}{r}\int_0^\infty \frac{1}{2\pi} H(t) \left[\tilde{G}^{\delta}_{xxH}(k_x,z,t) - \tilde{G}^{\delta}_{yyH}(k_x,z,t)\right] J_1(k_x r) dk_x \tag{5}$$

$$g_{zrH}(r,z,t) = -\frac{1}{i}\int_0^\infty \frac{1}{2\pi} H(t) \tilde{G}^{\delta}_{zxH}(k_x,z,t) k_x J_1(k_x r) dk_x \tag{6}$$

$$g_{zzH}(r,z,t) = \int_0^\infty \frac{1}{2\pi} H(t) \tilde{G}^{\delta}_{zzH}(k_x,z,t) k_x J_0(k_x r) dk_x \tag{7}$$

being J_n the Bessel function of the first kind and order n, and $\tilde{G}^{\delta}_{yyH}$ and $\tilde{G}^{\delta}_{mnH}$ are defined as:

$$\tilde{G}^{\delta}_{yyH}(k_x,z,t) = \frac{e^{-\xi_H k_x c_{sH} t}}{c_{sH}\rho_H} J_0\left(k_x c_{sH}\sqrt{1-\xi_H^2}\sqrt{t^2-t_s^2}\right) \tag{8}$$

$$\tilde{G}^{\delta}_{mnH}(k_x,z,t) = \frac{e^{-\xi_H k_x c_{sH} t}}{c_{sH}\rho_H} \left[R_{mn}(k_x,z,t)) - B_{mn}(k_x,z,t)\right] \qquad m,n = x,z \tag{9}$$

where $R_{mn}(k_x,z,t)$ is the Rayleigh pole term, $B_{mn}(k_x,z,t)$ is a branch-cut integral [21], and δ means response to an impulsive load.

Park and Kausel [21] separated the branch-cut integrals in three intervals: $1 \to \sqrt{2}$, $\sqrt{2} \to a$, and $a \to \infty$, where $a = c_{pH}/c_{sH}$. Moreover, they replaced the kernels by their asymptotes from $3a$. Thus, they computed the branch-cut integrals from the sum of their values in the following intervals: $1 \to \sqrt{2}$, $\sqrt{2} \to a$, $a \to 3a$, and $3a \to \infty$.

In this work, it is proposed to separate the branch-cut integrals in two intervals to reduce computational time: $1 \to a$ and $a \to \infty$. The kernels are also replaced by their asymptotes but, in the present methodology, from $5a$. Therefore, the branch-cut integrals are evaluated from the sum of their values in the intervals: $1 \to a$, $a \to 5a$, and $5a \to \infty$. The kernels of the integrals are expressed in a dimensionless form, and the integrals from $1 \to a$, and from $a \to 5a$, are numerically evaluated and saved in a table. The integrals from $5a \to \infty$ are analytically evaluated. This methodology allows to compute the branch-cut integrals with a numerical error lower than 0.25%.

The response of the layered half-space in the wavenumber-time domain for a point located at the layers is obtained as [19, 20]:

$$\tilde{g}_{kl}(k_x,z,t) = \tilde{G}_{klL}(k_x,z,z',t) * \frac{1}{2\pi} H(t) - \tilde{G}_{klL}(k_x,z,0,t) * \tilde{\tau}(k_x,t) \tag{10}$$

where $\tilde{G}_{klL}(k_x,z,z',t)$ is the response of the layer at z due to an Heaviside load applied at z', $\tilde{\tau}(k_x,t)$ are the tractions at the bottom interface which coincides with the top of the half-space, and $*$ means time convolution process. The origin of coordinates, i.e. $z = 0$, is placed at the top of the half-space.

The Green's functions for the layers $\tilde{G}_{klL}(k_x, z, z', t)$ are obtained from a modal superposition with the normal modes of the layer:

$$\tilde{G}_{klL}(k_x, z, z', t) = \sum_{j=1}^{\infty} e^{-\xi_{jL}\omega_{jL}t} \frac{\sin \omega_{djL} t}{\omega_{djL}} \phi_{jL}(k_x, z)\phi_{jL}(k_x, z') \tag{11}$$

The characteristic modal frequencies ω_{jL} and the corresponding modal shapes ϕ_{jL} are computed by making use of the Thin-Layer Method (TLM). The damped modal frequency is obtained from $\omega_{djL} = \omega_{jL}\sqrt{1-\xi_{jL}^2}$, where ξ_{jL} is the damping ratio of the layer.

Tractions at the bottom interface $\tilde{\tau}(k_x, t)$ are obtained from the compatibility of displacements and equilibrium of forces at $z = 0$, i.e., the interface between the layer and the half-space. The response at the interface of the half-space is computed as:

$$\tilde{g}_{kl}(k_x, 0, t) = \tilde{g}_{klH}(k_x, 0, t) * \tilde{\tau}(k_x, t) \tag{12}$$

The response at the bottom interface of the layer can be obtained from:

$$\tilde{g}_{kl}(k_x, 0, t) = \tilde{G}_{klL}(k_x, 0, z', t) * \frac{1}{2\pi} H(t) - \tilde{G}_{klL}(k_x, 0, 0, t) * \tilde{\tau}(k_x, t) \tag{13}$$

Equations (12) and (13) allow to evaluate the tractions $\tilde{\tau}(k_x, t)$. Finally, the response in the space-time domain is obtained from the inverse Hankel transform as [19, 20]:

$$g_{rr}(r, z, t) = \int_0^{\infty} \frac{1}{4\pi}(\tilde{g}_{xx}(k_x, z, t) + \tilde{g}_{yy}(k_x, z, t))k_x J_0(k_x r)dk_x - \tag{14}$$

$$\int_0^{\infty} \frac{1}{4\pi}(\tilde{g}_{xx}(k_x, z, t) - \tilde{g}_{yy}(k_x, z, t))k_x J_2(k_x r)dk_x \tag{15}$$

$$g_{rz}(r, z, t) = -i \int_0^{\infty} \frac{1}{2\pi} \tilde{g}_{xz}(k_x, z, t)k_x J_0(k_x r)dk_x \tag{16}$$

$$g_{\theta\theta}(r, z, t) = -\int_0^{\infty} \frac{1}{4\pi}(\tilde{g}_{xx}(k_x, z, t) + \tilde{g}_{yy}(k_x, z, t))k_x J_0(k_x r)dk_x - \tag{17}$$

$$\int_0^{\infty} \frac{1}{4\pi}(\tilde{g}_{xx}(k_x, z, t) - \tilde{g}_{yy}(k_x, z, t))k_x J_2(k_x r)dk_x \tag{18}$$

$$g_{zr}(r, z, t) = -i \int_0^{\infty} \frac{1}{2\pi} \tilde{g}_{zx}(k_x, z, t)k_x J_1(k_x r)dk_x \tag{19}$$

$$g_{zz}(r, z, t) = i \int_0^{\infty} \frac{1}{2\pi} \tilde{g}_{zz}(k_x, z, t)k_x J_0(k_x r)dk_x \tag{20}$$

Integration kernels appear in Equations (14-20) are smooth and they have not any singularities. The time step should be shorter than the shortest characteristic period of the system layers for stable computations [19, 20].

The fundamental solution is computed considering the cylindrical coordinate system as:

$$\mathbf{g}^{cyl}(r, z, t) = \begin{bmatrix} g_{rr} & 0 & g_{rz} \\ 0 & g_{\phi\phi} & 0 \\ g_{zr} & 0 & g_{zz} \end{bmatrix} \tag{21}$$

Equation (21) represents an antisymmetrical second order tensor. The fundamental solution in the cartesian coordinate system is obtained transforming the Equation (21) as follows:

$$\mathbf{g}(x, y, z, t) = \mathbf{\Omega}\mathbf{g}^{cyl}\mathbf{\Omega}^T \tag{22}$$

where $\mathbf{\Omega}$ is the transformation matrix from cylindrical to cartesian coordinate system:

$$\mathbf{\Omega} = \begin{bmatrix} \cos\phi & \sin\phi & 0 \\ -\sin\phi & \cos\phi & 0 \\ 0 & 0 & 1 \end{bmatrix} \tag{23}$$

Following, the response of a homogeneous and a layered half-space due to a Heaviside point load is studied to validate the proposed methodology. Since analytical solutions of both problems are not available, the MATLAB toolbox EDT 2.1 [26, 27] based on the direct stiffness method [6] in the wavenumber-frequency domain is used to validate the results obtained from the proposed methodology. Moreover, numerical results are also verified by comparison with the explicit displacement solution for a Heaviside load applied at the surface of a homogeneous elastic half-space presented recently by Kausel [23].

First, a homogeneous half-space was assumed with the following properties: $c_{pH} = 300\,\text{m/s}$, $c_{sH} = 150\,\text{m/s}$, $\xi_H = 0.05$, and $\rho_H = 2000\,\text{kg/m}^3$. Figure 2 shows the fundamental solution for displacements at the half-space surface at distance $r = 10\,\text{m}$ from the source. The response shows an initial perturbation at the arrival time of the P-wave ($t = r/c_{pH}$) which it can be clearly identified in the Figures 2.(a,b) where a horizontal load is considered. The maximum displacement is reached between the arrival time of S-wave ($t = r/c_{sH}$) and the arrival time of Rayleigh wave.

The agreement between the computed results and those obtained from EDT 2.1 toolbox [26] is quite good. The mismatches with the analytical solution [23] are due to the internal soil damping induces a smoother behaviour around the different arrival time of the waves.

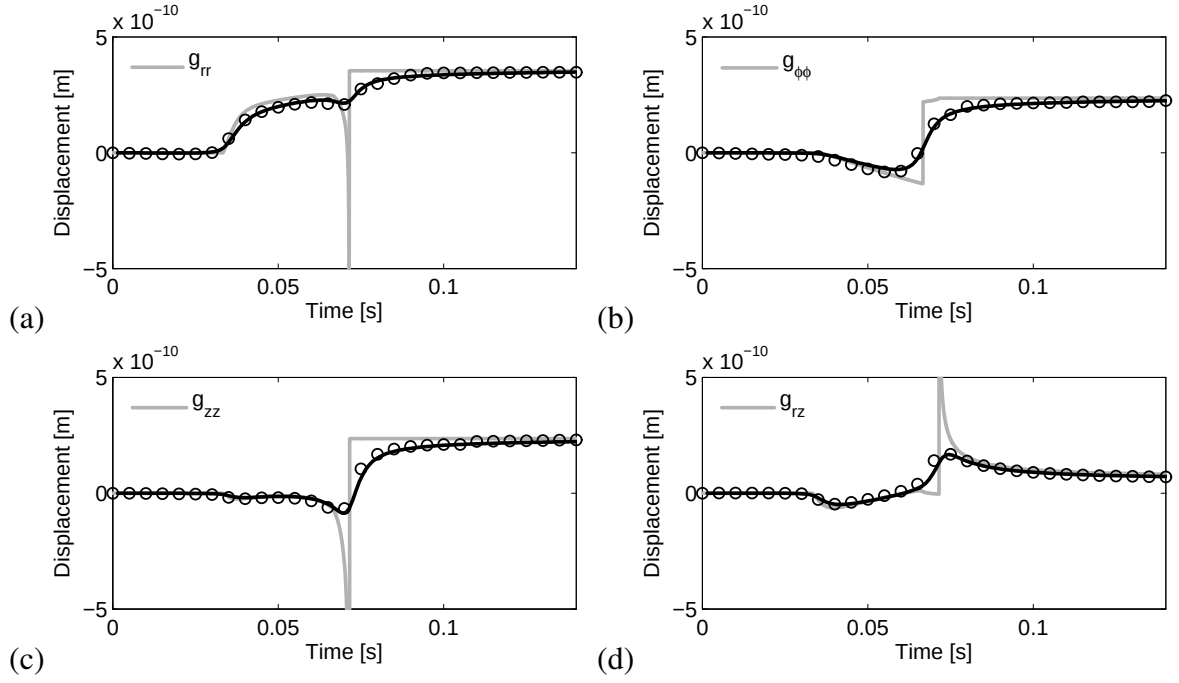

Figure 2: (a) Radial and (b) tangential, and (c) vertical and (d) radial displacements due to a (a,b) horizontal and (c,d) vertical Heaviside load applied at the surface of a homogeneous half-space for a point located at the surface at $r = 10\,\text{m}$ from the source: analytical solution [23] (grey line), EDT 2.1 toolbox [26] (black line) and proposed methodology (black circles).

Next, the response of a layered half-space is studied. A layer with a thickness $h_L = 5\,\text{m}$, and $c_{pL} = 300\,\text{m/s}$, $c_{sL} = 150\,\text{m/s}$, $\xi_L = 0.05$, and $\rho_L = 2000\,\text{kg/m}^3$, on top of a half-space with $c_{pH} = 600\,\text{m/s}$, $c_{sH} = 300\,\text{m/s}$, $\xi_H = 0.05$, and $\rho_H = 2000\,\text{kg/m}^3$ is considered. Figure 3 shows the displacements at a point of the soil surface due to horizontal and vertical loads, and they are compared with the analytical solution for a homogeneous half-space with the same properties that the upper layer of the soil. The mismatches between the numerical results can be neglected. It can be observed in Figure 3 the influence of the soil stratification on the wave propagation from the comparison with the analytical solution for a homogeneous half-space.

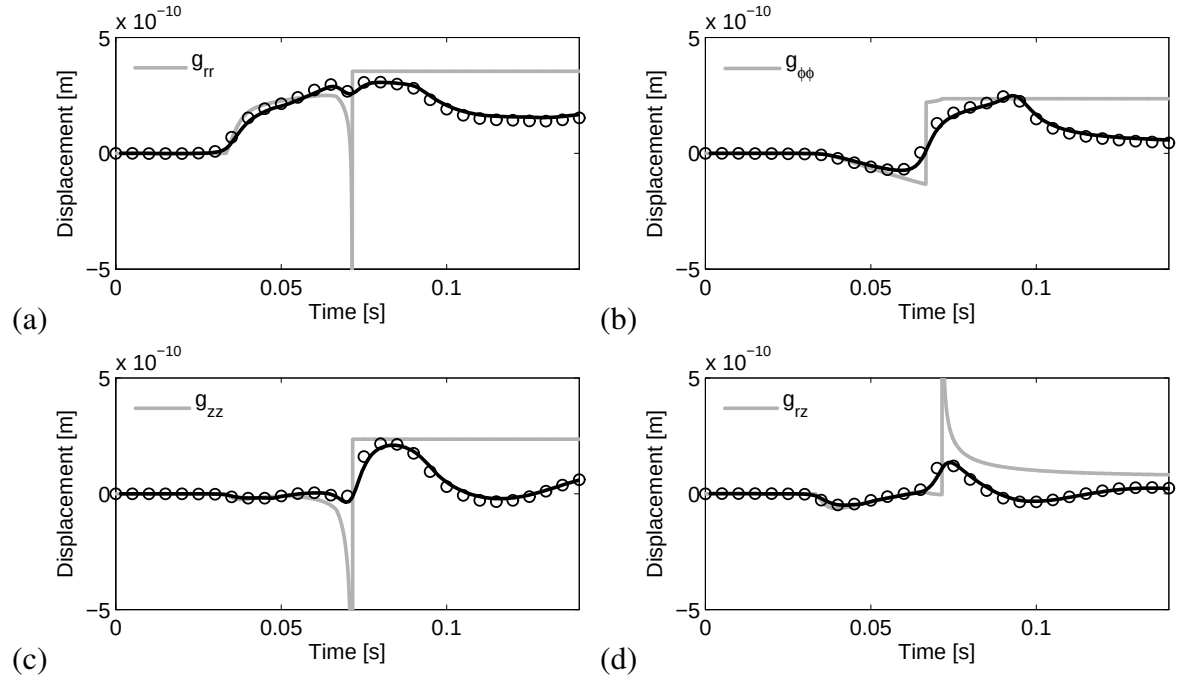

Figure 3: (a) Radial and (b) tangential, and (c) vertical and (d) radial displacements due to a (a,b) horizontal and (c,d) vertical Heaviside load applied at the surface of a layered half-space for a point located at the surface at $r = 10\,\text{m}$ from the source: analytical solution [23] (grey line), EDT 2.1 toolbox [26] (black line) and proposed methodology (black circles).

3 Boundary element formulation

This section presents the three-dimensional (3D) boundary element formulation in time domain based on the half-space fundamental solution previously developed. The integral representation of the displacement u^i for a point i on the soil surface at time t, with zero body forces and zero initial conditions can be written as [3]:

$$\begin{aligned} c_{lk}^i u_k^i(\mathbf{x}^i, t) = &\int_0^{t+} \int_\Gamma u_{lk}^*(\mathbf{x}, t-\tau; \mathbf{x}^i) p_k(\mathbf{x}, \tau) d\Gamma d\tau \\ &- \int_0^{t+} \int_\Gamma p_{lk}^*(\mathbf{x}, t-\tau; \mathbf{x}^i) u_k(\mathbf{x}, \tau) d\Gamma d\tau \end{aligned} \tag{24}$$

where u_k and p_k stand for the k component of the displacement and traction, respectively; $u_{lk}^*(\mathbf{x}, t-\tau; \mathbf{x}^i)$ and $p_{lk}^*(\mathbf{x}, t-\tau; \mathbf{x}^i)$ are the half-space fundamental solution displacement and

traction tensors, respectively, at point $\mathbf{x}$ due to an impulsive load applied at $\mathbf{x}^i$ in l direction. The integral-free term c^i_{lk} depends only on the boundary geometry at point $\mathbf{x}^i$, and its value is unitary at the soil surface for a smooth boundary. For non-smooth boundaries c^i_{lk} is computed as presented in Reference [24].

Half-space fundamental solution for an impulsive load is derived from the solution for a Heaviside load as:

$$u^*_{lk}(\mathbf{x}, t; \mathbf{x}^i) = \frac{\partial g_{lk}(\mathbf{x}, t; \mathbf{x}^i)}{\partial t} \tag{25}$$

$$p^*_{lk}(\mathbf{x}, t; \mathbf{x}^i) = \frac{\partial f_{lk}(\mathbf{x}, t; \mathbf{x}^i)}{\partial t} \tag{26}$$

where the traction solution, f_{lk}, is evaluated using the constitutive law for a linear elastic, homogeneous and isotropic solid by computing the spatial derivatives of the Green's function.

Displacements and tractions over the boundary are approximated at the time step $t = n\Delta t$ from their nodal values u^{mj}_k and p^{mj}_k, using the space interpolation functions $\phi^j(r)$ and $\psi^j(r)$, and the time interpolation functions $\eta^m(\tau)$ and $\mu^m(\tau)$ as:

$$\begin{aligned} c^i_{lk} u^i_k(\mathbf{x}^i, t) = \sum_{m=1}^{n} \sum_{j=1}^{Q} \Bigg\{ & \left[\int_{\Gamma_j} \int_{\Delta t_m} u^*_{lk}(\mathbf{x}, t-\tau; \mathbf{x}^i) \mu^m d\tau \psi^j \, d\Gamma \right] p^{mj}_k \\ & - \left[\int_{\Gamma_j} \int_{\Delta t_m} p^*_{lk}(\mathbf{x}, t-\tau; \mathbf{x}^i) \eta^m d\tau \phi^j \, d\Gamma \right] u^{mj}_k \Bigg\} \end{aligned} \tag{27}$$

where Q is the total number of boundary nodes and Γ_j represents the elements to which node j belongs.

Time kernels in Equation (27) are analytically integrated using constant and linear piecewise time interpolation functions $\mu^m(\tau)$ and $\eta^m(\tau)$ for tractions and displacements, respectively:

$$\begin{aligned} U^{nm}_{lk} &= \int_{\Delta t_m} u^*_{lk}(\mathbf{x}, t-\tau; \mathbf{x}^i) \mu^m d\tau \\ &= g_{lk}(\mathbf{x}, [n-m+1]\Delta t; \mathbf{x}^i) - g_{lk}(\mathbf{x}, [n-m]\Delta t; \mathbf{x}^i) \end{aligned} \tag{28}$$

$$\begin{aligned} P^{nm}_{lk} = \int_{\Delta t_m} p^*_{lk}(\mathbf{x}, t-\tau; \mathbf{x}^i) \eta^m d\tau = 1/\Delta t \, \big\{ & F_{lk}(\mathbf{x}, [n-m+1]\Delta t; \mathbf{x}^i) \\ -2F_{lk}(\mathbf{x}, [n-m]\Delta t; \mathbf{x}^i) + & F_{lk}(\mathbf{x}, [n-m-1]\Delta t; \mathbf{x}^i) \big\} \end{aligned} \tag{29}$$

where $\mathbf{F}(\mathbf{x}, t; \mathbf{x}^i)$ is the time integral of the traction tensor $\mathbf{f}(\mathbf{x}, t; \mathbf{x}^i)$.

After interpolating the boundary variables, the integral equation (27) becomes:

$$c^i_{lk} u^i_k(\mathbf{x}^i, t) = \sum_{m=1}^{n} \sum_{j=1}^{Q} \left\{ \left[\int_{\Gamma_j} U^{nm}_{lk} \psi^j \, d\Gamma \right] p^{mj}_k - \left[\int_{\Gamma_j} P^{nm}_{lk} d\tau \phi^j \, d\Gamma \right] u^{mj}_k \right\} \tag{30}$$

Equation (30) is written in a more compact form as:

$$c^i_{lk} u^{ni}_k = \sum_{m=1}^{n} \sum_{j=1}^{Q} \left[G^{nmij}_{lk} p^{mj}_k - \widehat{H}^{nmij}_{lk} u^{mj}_k \right] \tag{31}$$

Once the integral-free term c_{lk}^{i} is included in the system matrix, the integral representation for point i at time $t = n\Delta t$ becomes:

$$\mathbf{H}^{nn}\mathbf{u}^{n} = \mathbf{G}^{nn}\mathbf{p}^{n} + \sum_{m=1}^{n-1}\left[\mathbf{G}^{nm}\mathbf{p}^{m} - \mathbf{H}^{nm}\mathbf{u}^{m}\right] \tag{32}$$

where H_{lk}^{nmij} collects for c_{lk}^{i} when $i = j$ and $n = m$.

In this work nine-node rectangular quadratic boundary elements are used. Identical space interpolation shape functions $\phi^{j}(r)$ and $\psi^{j}(r)$ are assumed. The spatial integration is done only in those parts of an element under the effects of the fundamental solution waves, according to the causality condition of each term of the fundamental solution [25]. Each side of the element is divided into equal parts in the natural coordinate domain yielding an element subdivision.

Equation (32) yields a system of equations that is solved step by step to obtain the time variation of displacements and tractions at the boundary. After boundary unknowns are solved, the radiated wave field $\mathbf{u}_{r}^{n}$ at any internal point or at the free field is computed by means of the integral representation of the Somigliana identity:

$$\mathbf{u}_{r}^{n} = \sum_{m=1}^{n}\left(\mathbf{G}_{r}^{nm}\mathbf{p}^{m} - \widehat{\mathbf{H}}_{r}^{nm}\mathbf{u}^{m}\right) \tag{33}$$

where $\mathbf{G}_{r}^{nm}$ and $\widehat{\mathbf{H}}_{r}^{nm}$ are the boundary element matrices computed considering only domain point as source points.

The proposed BEM formulation is verified analysing the response of a homogeneous and a layered half-space due to a vertical impulsive point load. The half-space's properties were indicated in Section 2.

Figure 4 shows the vertical and radial response due to a impulsive vertical load at a point of the half-space surface at $r = 10$ m from the source. In this figure can be observed the dispersive character of the wave propagation in the layered half-space mainly for the response at times higher than $t = r/c_{sL}$. The agreement between the computed results and those obtained from EDT 2.1 [26] toolbox is again quite good.

4 Coupled BEM-FEM formulation

This work uses the `SSIFiBo` toolbox[1] for `MATLAB` previously developed by Galvín and Romero [8, 18, 28]. The SSI problem is decomposed in two subdomains represented by the BEM and the FEM. The FEM module of the toolbox does not include any pre-processor. Instead, a gateway for commercial software allows importing directly the structure model. Coupling of both methods requires that the equilibrium of forces and the compatibility of displacements are fulfilled at the interface between the two subdomains. The coupling is performed directly and the equations of both subdomains are assembled into a global system of equations. The FEM equation is solved at each time step following an implicit time integration GN22 Newmark method [4, 29].

5 Experimental study

In this section, the proposed BEM-FEM model is experimentally validated by the measurements recorded at a site located at León, Spain. The dynamic soil characteristics at the measurement site were identified by means of a Spectral Analysis of Surface Waves test (SASW).

[1] http://personal.us.es/pedrogalvin/ssifibo.en.html

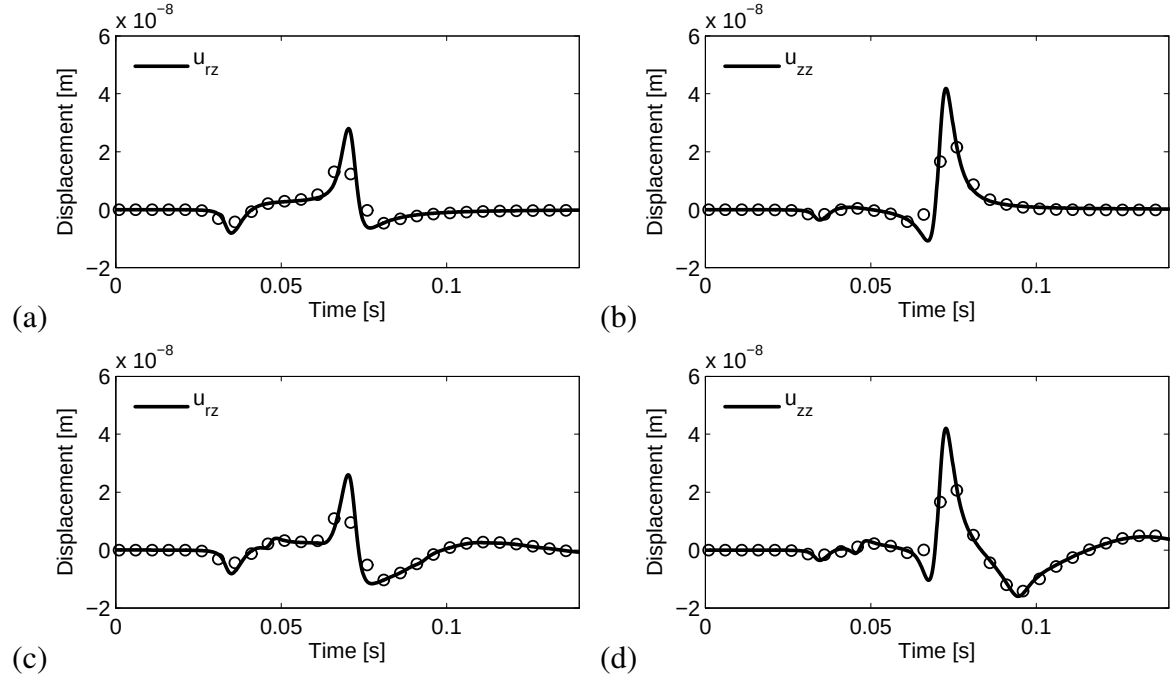

Figure 4: (a,c) Radial and (b,d) vertical displacement due to an impulsive vertical load applied at the surface of a (a,b) homogeneous and (c,d) layered half-space for a point located at the surface at $r = 10\,\mathrm{m}$ from the source: EDT 2.1 toolbox [26] (black line) and proposed method (black circles).

The vertical free field response due to hammer impacts applied to a $0.5\,\mathrm{m} \times 0.5\,\mathrm{m} \times 0.08\,\mathrm{m}$ aluminium foundation was measured using accelerometers located at the soil's surface (Figure 6.(a)). The load was measured by means of a force sensor in the hammer. Figure 6.(b) shows one of the accelerometers used to measure the free field response. Figure 5 shows the location of the aluminium foundation and the measurement line.

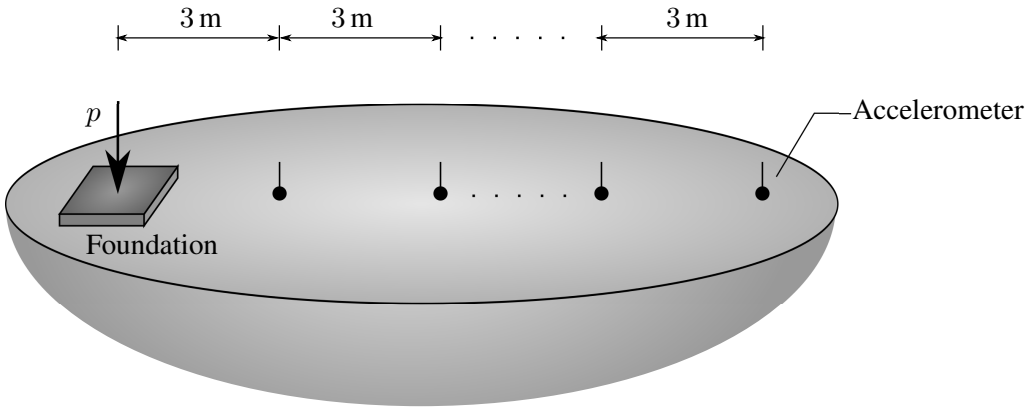

Figure 5: Location of foundation and accelerometers.

The shear wave velocity profile was identified from the SASW test by fitting the computed dispersion curve to the experimental dispersion curve of the fundamental Rayleigh wave at the site [30]. The results show that the soil can be represented by a single layer with a thickness $h_L = 4.1\,\mathrm{m}$ and a shear wave velocity $c_{sL} = 150\,\mathrm{m/s}$ on a half-space with a shear wave velocity $c_{sH} = 495\,\mathrm{m/s}$. A value of $1900\,\mathrm{kg/m^3}$ is assumed for the density of the layer and the half-

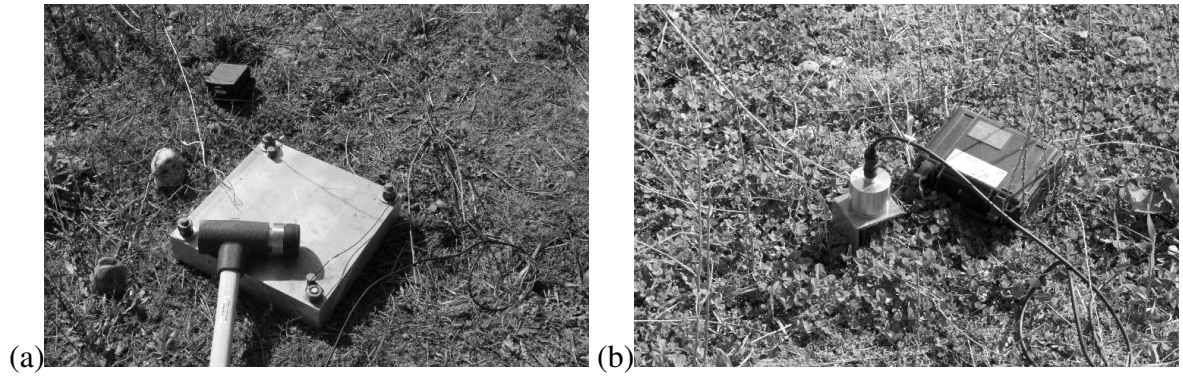

Figure 6: (a) Aluminium foundation and impact hammer and (b) accelerometer anchored in the soil surface.

space. Poisson's ratio has been estimated from the geophysical tests as $\nu = 0.4$. For both, the layer and the half-space, a value of 0.06 was assumed for the material damping ratio ξ. The density was estimated from the geotechnical investigation. Its high value could be due to the soil was saturated. The dynamic soil characteristics are summarized in table 1.

	h [m]	c_p [m/s]	c_s [m/s]	ξ [-]	ν [-]	ρ [kg/m^3]
Layer	4.1	367	150	0.06	0.4	1900
Half-space	∞	1212	495	0.06	0.4	1900

Table 1: Dynamic soil characteristics.

The SASW test was modelled by the proposed numerical model. Figure 7 shows the discretization that it was used to compute the vertical soil displacements. The $0.08\,$m thick aluminium foundation was represented by 4 eight-node solid elements. The aluminium material had the following properties: Young's modulus $E = 70 \times 10^9\,$N/m^2, Poisson's ratio $\nu = 1/3$ and density $\rho = 2700\,$kg/m^3. The soil was represented as a layered half-space according to Table 1. Soil discretization extends only to soil-foundation interface using one nine-node rectangular quadratic boundary elements. A time step $\Delta t = 1 \times 10^{-3}\,$s was chosen according to the soil properties to ensure the stability of the methodology.

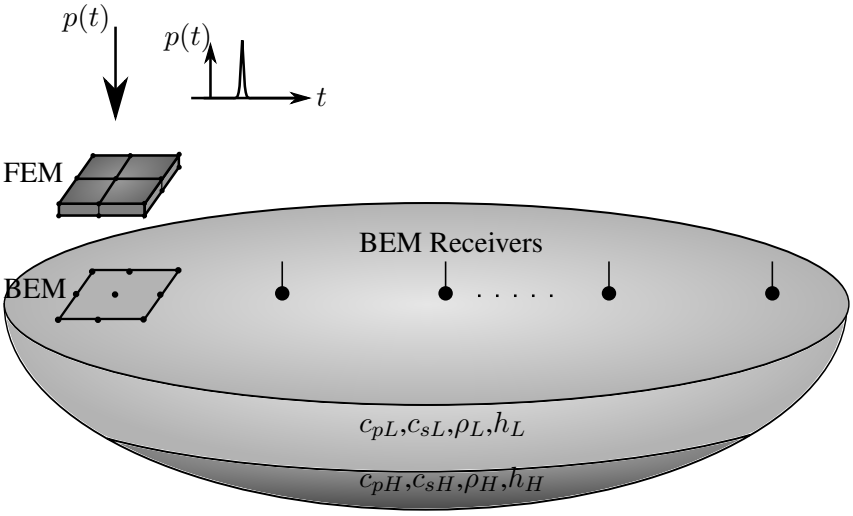

Figure 7: Soil-foundation discretization.

Figure 8 shows the experimental and numerical vertical soil displacements at points located

at the soil surface from 3 m to 24 m form the foundation. The signal period as well as its peak value correspond relatively well. However, the agreement between numerical and experimental results is not perfect, and it is required a more comprehensive analysis to explain the mismatches. Therefore, results in the frequency domain were computed.

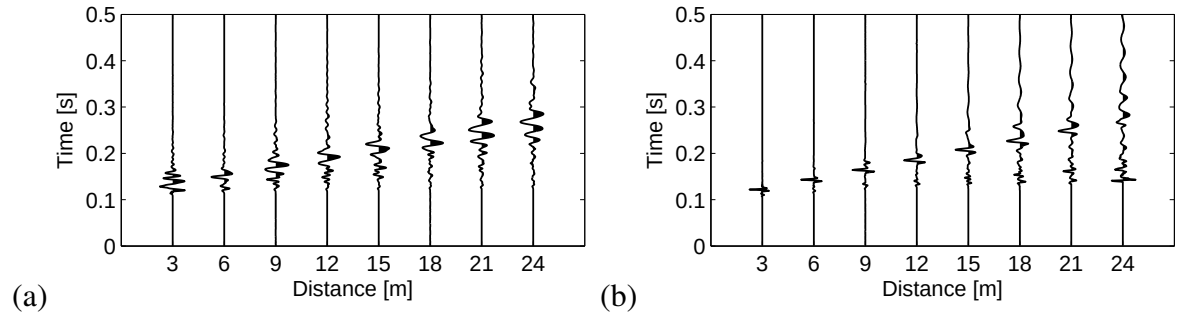

Figure 8: Free field acceleration due to a Ricker pulse: (a) experimental and (b) numerical results.

The transfer function was obtained by the Fourier transform from the numerical and experimental results as [26]:

$$\widehat{H}(r,\omega) = \frac{\widehat{A}(r,\omega)}{\widehat{F}(r,\omega)} \tag{34}$$

where $\widehat{A}(r,\omega)$ and $\widehat{F}(r,\omega)$ mean the soil acceleration and the applied load in the frequency domain.

Figure 9 shows the frequency response function at several points located at the soil surface. At points located at 3 m, 6 m and 9 m from source, a relatively good agreement was obtained between the experimental records and the numerical results for frequencies below 70 Hz, but the response was overestimated above 70 Hz. At larger distances from the source, the numerical results underestimates the measured value at the frequency range between 20 Hz and 50 Hz. This could be due to uncertain in the dynamic soil properties identification for higher frequencies.

Finally, results in the wavenumber-frequency domain were also obtained. The response in the wavenumber-frequency domain was computed by a Hankel transform as:

$$\widetilde{H}(k_r,\omega) = \int_0^\infty \widehat{H}(r,\omega) J_0(k_r,\omega) r dr \tag{35}$$

Figure 10 shows the resulting experimental and numerical wavenumber-frequency spectrum $\widetilde{H}(k_r,\omega)$ in terms of the phase velocity ω/k_r. The maxima in the wavenumber-frequency spectrum are due to the Rayleigh waves and they allow to estimate the dispersion curve. It can be observed from Figure 10.(a) that the experimental dispersion curve at a range from 12 Hz to 67 Hz was well-estimated. However, experimental records at frequencies below 8 Hz, and above 70 Hz are affected by noise. Figure 10.(b) shows the numerical wavenumber-frequency spectrum which it is only correlated with the experimental results in the previously indicated frequency range.

The mismatches between numerical and experimental results could be explained by this analysis.

6 Numerical example

In this section, the dynamic behaviour of a framed wall building subjected to a uniform incident wave field is studied. The analysis of the wave propagation problem is done by decom-

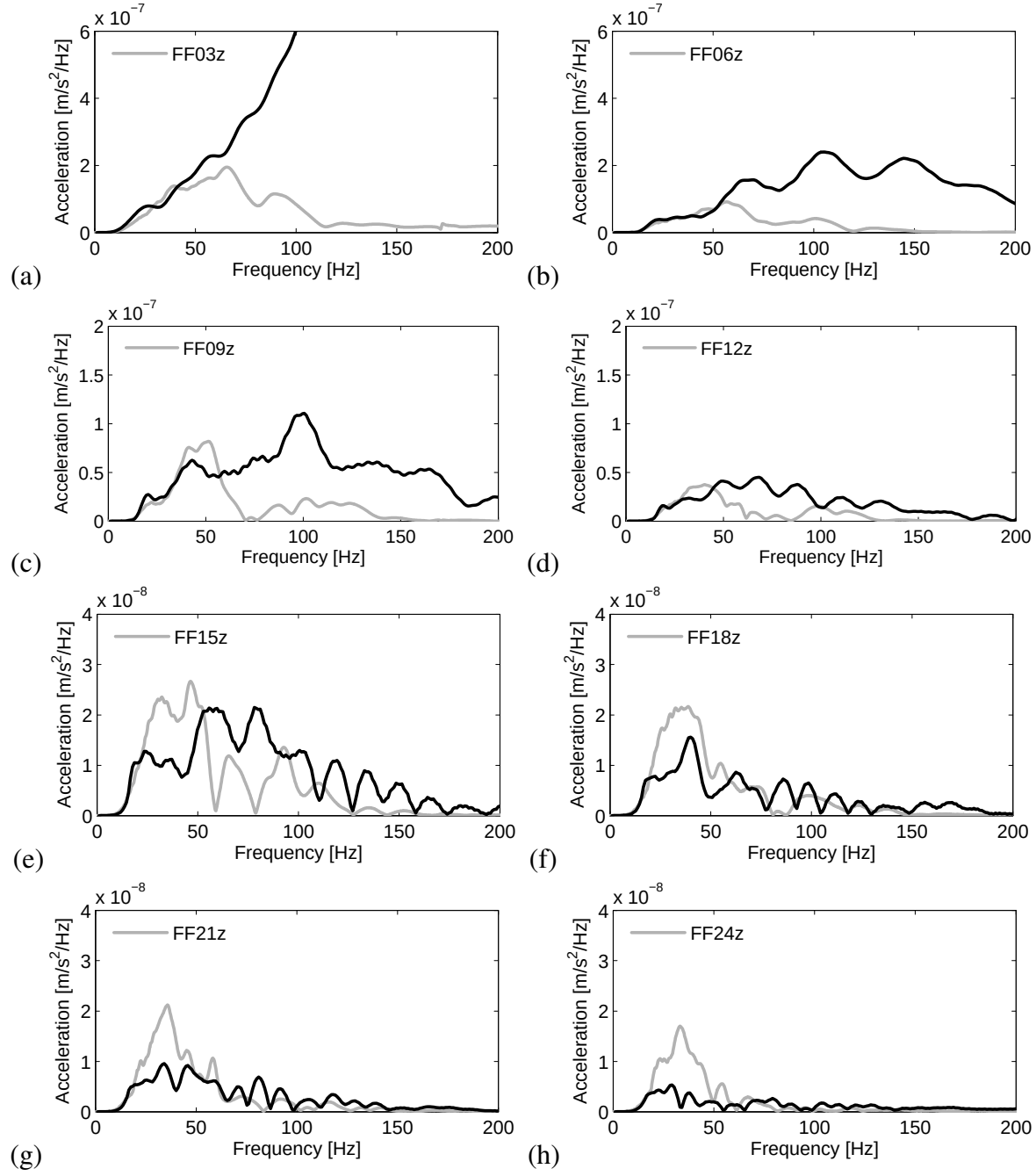

Figure 9: Free field frequency response function at (a) 3 m, (b) 6 m, (c) 9 m, (d) 12 m, (e) 15 m, (f) 18 m, (g) 21 m, and (h) 24 m, from the load: experimental (grey line) and numerical results (black line).

position of the total wave field in two terms: the incident and the scattered fields [3]. The wave propagation is solved by Equation (32). Once the scattered wave field is obtained, the incident wave field is superimposed to the radiation problem (Equation (33)).

The dimensions of the studied twelve-storey building were $12\,\text{m} \times 12\,\text{m} \times 36\,\text{m}$ (Figure 11). The structure consisted of eight concrete columns with $0.6\,\text{m} \times 0.4\,\text{m}$ section, four edge beams with $0.6\,\text{m} \times 0.2\,\text{m}$ section, and two framed concrete wall with $2.4\,\text{m} \times 0.15\,\text{m}$ section. The floors were simply supported concrete slabs with a thickness of $0.2\,\text{m}$. The floors consist of a two-dimensional frame with axial stiffness per unit length $EA = 1.433 \times 10^9$ N/m, bending stiffness

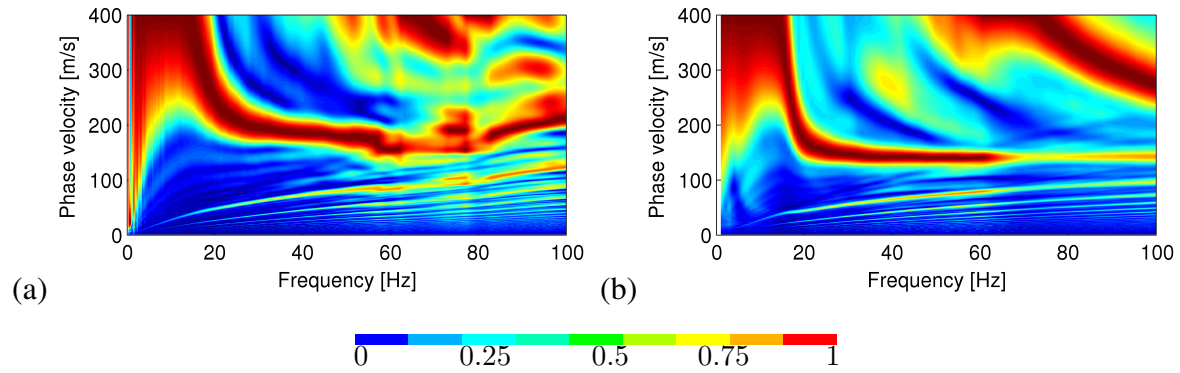

Figure 10: Frequency-wavenumber spectrum of the wave field: (a) experimental, and (b) numerical results.

per unit length $EI = 9.935 \times 10^6$ Nm, and a mass per unit area of $m = 172\,\text{kg/m}^2$. The structure was founded on a 1.0 m thick concrete slab. The concrete material had the following properties: Young's modulus $E = 20 \times 10^9\,\text{N/m}^2$, Poisson's ratio $\nu = 0.2$ and density $\rho = 2400\,\text{kg/m}^3$.

The structural damping was considered by a Rayleigh model [31]. The damping matrix, $\mathbf{C} = a_0\mathbf{M} + a_1\mathbf{K}$, was computed proportional to the mass, $\mathbf{M}$, and the stiffness, $\mathbf{K}$, matrices. A structural damping, $\zeta = 5\,\%$, was set for the first and second mode shapes. Proportional constant values were $a_0 = 0.4193\,\text{s}^{-1}$ and $a_1 = 0.0042\,\text{s}$.

The structure was discretized by 1248 two-node Euler-Bernoulli beam elements to represent columns and beams, and 3072 four-node shell elements for considering the floors and the framed walls. Figure 11.(b) shows the discretization of the building. The element size varies from 0.5 m to 1.25 m. This length was enough to represent adequately the structure dynamic behaviour.

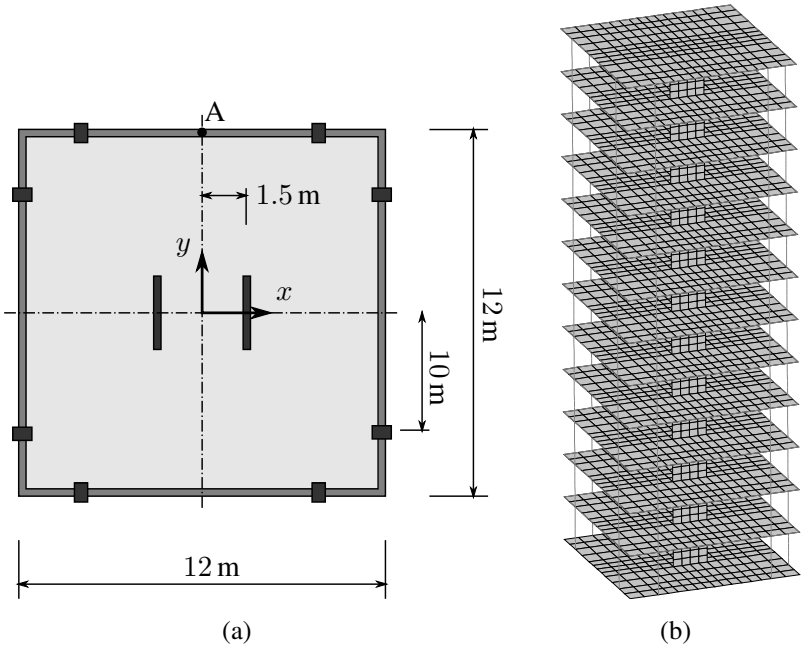

Figure 11: (a) Building plan geometry and (b) discretization.

Soil discretization extends only to soil-structure interface using 48 nine-node rectangular quadratic boundary elements. This problem was previously studied by Galvín and Romero [10] considering the soil as a homogeneous half-space. In this paper, two type of soils are

considered: a homogeneous half-space with $c_{pH} = 300\,\text{m/s}$, $c_{sH} = 150\,\text{m/s}$, $\xi_H = 0.05$, and $\rho_H = 1600\,\text{kg/m}^3$, and a layered half-space with the properties presented in Table 2. A time step $\Delta t = 4.50 \times 10^{-3}\,\text{s}$ was chosen according to each soil properties to ensure the stability of the methodology. Following, the computed results from both cases are compared.

	h [m]	c_p [m/s]	c_s [m/s]	ξ [-]	ρ [kg/m^3]
Layer	2	300	150	0.05	1600
Half-space	∞	600	300	0.05	1600

Table 2: Soil properties considered for the foundation of the building.

In this example, the building response due to a uniform incident wave field is analysed. The incident wave fields corresponded with plane SH propagating along x-axis. The incident waves induced an uniform acceleration at the soil-structure interface, $a(\mathbf{x}, t) = 1\delta(t)\,\text{m/s}^2$, where δ is the Dirac delta function.

Figure 12 shows the time history and frequency content of the horizontal displacement in the y-direction at the ground, and twelfth floors. Frequency response has been obtained by applying a direct Fourier Transform to the time history. Results for the observation point A (Figure 11.(a)) are shown. The floor response amplitudes increased with the level floor. The amplitudes decreased for the building founded on the layered half-space according to the higher stiffness.

The response for the building founded on the layered half-space shows two peaks at the resonance frequencies given by $f_1 = 0.83\,\text{Hz}$ and $f_2 = 2.89\,\text{Hz}$. These frequencies correspond with transversal mode shapes along y-direction. The fundamental period of the building was lightly higher for the homogeneous soil due its higher flexibility. At low frequencies the response is lower if the layered half-space is considered because the wavelength in the soil is large and the properties of the half-space are prevailing. At high frequencies, the wavelength is small compared to the thickness of the layer and the wave propagation in the soil is determined by the characteristics of the top layer.

Figure 13 shows the amplitude at the first resonance frequency at each floor for the different studied soil. The building response at the ground is similar for both considered cases. However, the soil flexibility caused a significantly increment of the amplitude with the story level.

7 Conclusions

This paper has developed a time domain BEM formulation using Green's function for a layered half-space as the fundamental solution. The layered half-space fundamental solution is advantageous because of soil discretization is limited to soil-structure interface and it allows easily considering soil stratification and material damping. The proposed fundamental solution has been verified by a benchmark problem.

The BEM formulation has been coupled with a FEM methodology to study soil-structure interaction problems. The obtained results have demonstrated that the influence of the soil stratification is large.

The proposed BEM-FEM numerical model has been applied to analysed actual ground vibrations. The methodology has been used to modelled a SASW test. The numerical results have been compared with the measured free field response.

The presented results show that the proposed methodology allows describing accurately the dynamic soil-structure interaction considering the influence of the soil stratification.

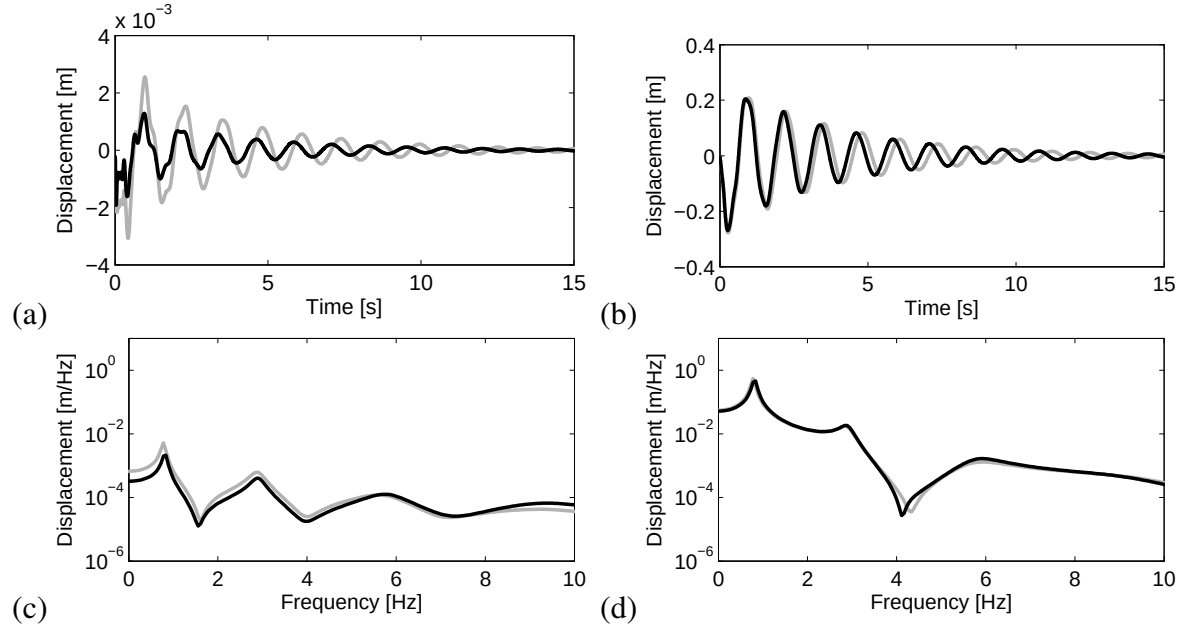

Figure 12: (a,b) Time history and (c,d) frequency content of the horizontal displacement along y-direction at the observation points A located at (a,c) ground floor and (b,d) 12^{th} floor, for a building founded on a homogeneous (grey line) and a layered half-space (black line).

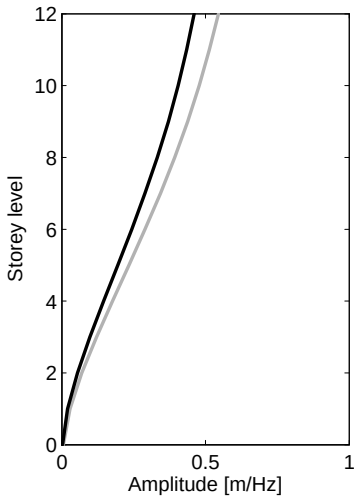

Figure 13: Maximum amplitude at the first resonance frequency at each floor, for a building founded on homogeneous (grey line) and layered half-space (black line).

Acknowledgments

This research was funded by the Spanish Ministry of Economy and Competitiveness (Ministerio de Economía y Competitividad) through research project BIA2013-43085-P. Financial support is gratefully acknowledged. The support given by the Andalusian Scientific Computing Centre (CICA) is also gratefully.

REFERENCES

[1] E. Kausel, Early history of soil-structure interaction. Soil Dynamics and Earthquake Engineering **30**(9), 822-832 (2010)

[2] A.C. Eringen, E.S. Suhubi, Elastodynamics, Volume 2, Linear theory. Academic Press, New York, USA (1975)

[3] J. Domínguez, Boundary elements in dynamics. Computational Mechanics Publications and Elsevier Aplied Science, Southampton (1993)

[4] O.C. Zienkiewicz, R.L. Taylor, The Finite Element Method, Volume I: The Basis. McGraw-Hill, New York (1967)

[5] J.J Aznárez, O. Maeso, J. Domínguez, BE analysis of bottom sediments in dynamic fluid-structure interaction problems. Engineering Analysis with Boundary Elements **30**(2), 124–136 (2006)

[6] E. Kausel, J.M. Roësset, Stiffness matrices for layered soils. Bulletin of the Seismological Society of America **71**, 1743–1761 (1981)

[7] S. François, L. Pyl, H.R. Masoumi, G. Degrande, The influence of dynamic soil-structure interaction on traffic induced vibrations in buildings. Soil Dynamics and Earthquake Engineering **27** 655–674 (2007).

[8] A. Romero, P. Galvín, J. Domínguez, 3D non-linear time domain FEM–BEM approach to soil–structure interaction problems. Engineering Analysis with Boundary Elements **37**(3), 501–512 (2013)

[9] C. Bode, R. Hirschauer, S.A. Savidis, Soil-structure interaction in the time domain using halfspace Green's functions. Soil Dynamics and Earthquake Engineering **22**(4), 283–295 (2002)

[10] P. Galvín, A. Romero, A 3D time domain numerical model based on half-space Green's function for soil-structure interaction analysis. Computational Mechanics **53**, 1073–1085 (2014)

[11] A.M. Kaynia, E. Kausel, Dynamics of piles and pile groups in layered soil media. Soil Dynamics and Earthquake Engineering **10**(8) 386–401 (1991)

[12] G. Lombaert, G. Degrande, D. Clouteau, The influence of the soil stratification on free field traffic-induced vibrations. Archive of Applied Mechanics **71** 661–678 (2001)

[13] L. Auersch, The effect of critically moving loads on the vibrations of soft soils and isolated railway tracks. Journal of Sound and Vibration **310**(3) 587–607 (2008)

[14] L. Auersch, Train induced ground vibrations: different amplitude-speed relations for two layered soils. Proceedings of the Institution of Mechanical Engineers, Part F: Journal of Rail and Rapid Transit **226**(5) 469–488 (2012)

[15] S. François, M. Schevenels, P. Galvín, G. Lombaert, G. Degrande, A 2.5D coupled FE-BE methodology for the dynamic interaction between longitudinally invariant structures and a layered halfspace. Computer Methods in Applied Mechanics and Engineering **199** 1536–1548 (2010)

[16] P. Galvín, S. François, M. Schevenels, E. Bongini, G. Degrande, G. Lombaert, A 2.5D coupled FE-BE model for the prediction of railway induced vibrations. Soil Dynamics and Earthquake Engineering **30** 1500–1512 (2010).

[17] D.C. Rizos, Z. Wang, Coupled BEM-FEM solutions for direct time domain soil-structure interaction analysis. Engineering Analysis with Boundary Elements **26**, 877–888 (2002)

[18] P. Galvín, A. Romero, J. Domínguez, Fully three-dimensional analysis of high-speed train-track-soil-structure dynamic interaction. Journal of Sound and Vibration **329**(24), 5147–5163 (2010)

[19] J. Park, E. Kausel, Response of layered half-space obtained directly in the time domain, Part I: SH sources. Bulletin of the Seismological Society of America **96**, 1725–1809 (2006)

[20] E. Kausel, J. Park, Response of layered half-space obtained directly in the time domain, Part II: SV-P and Three-Dimensional sources Bulletin of the Seismological Society of America **96**, 1810–1826 (2006)

[21] E. Kausel, J. Park, Impulse response of elastic half-space in the wavenumber-time domain. Journal of Engineering Mechanics, ASCE **130**(10) 1211–1222 (2004)

[22] J. Park, Wave Motion in finite and infinite media using the Thin-Layer Method. PhD thesis. Massachusetts Institute of Technology, Department of Civil and Environmental Engineering (2002)

[23] E. Kausel, Lamb's problem at its simplest. Proceedings of the Royal Society A: Mathematical, Physical and Engineering Sciences 469:20120462

[24] V. Mantic, A new formula for the C-matrix in the Somigliana identity. Journal of Elasticity **33**(3), 191–201 (1993)

[25] P. Galvín, J. Domínguez, Analysis of ground motion due to moving surface loads induced by high-speed trains. Engineering Analysis with Boundary Elements **31**(11), 931–941 (2007)

[26] M. Schevenels, S. François, G. Degrande, EDT: An ElastoDynamics Toolbox for MATLAB. Computers & Geosciences **35**(8) 1752–1754 (2009)

[27] M. Schevenels, G. Degrande, S. François, EDT: An ElastoDynamics Toolbox for MATLAB. Proceedings of the Inaugural International Conference of the Engineering Mechanics Institute (EM08), Minneapolis, Minnesota, U.S.A., (2008).

[28] P. Galvín, A. Romero:, A MATLAB toolbox for soil-structure interaction analysis with finite and boundary elements. Soil Dynamics and Earthquake Engineering **57**, 10–14 (2014)

[29] N.M. Newmark, A method of computation for structural dynamics. ASCE Journal of the Engineering Mechanics Division **85**(1), 67–94 (1959)

[30] ADIF, Estudio vibratorio. Línea de alta velocidad Madrid-Asturias. Tramo: Palencia-León. Technical report (in Spanish), (2009)

[31] R.W. Clough, J. Penzien, Dynamic of Structures. McGraw-Hill, New York (1975)